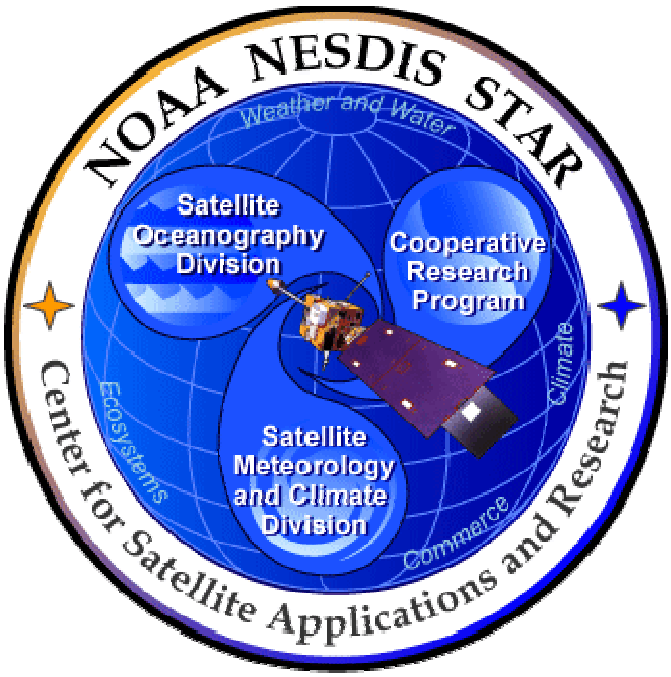

NOAA NESDIS
CENTER for SATELLITE APPLICATIONS and RESEARCH

GOES-R Advanced Baseline Imager (ABI) Algorithm Theoretical Basis Document For Absorbed Shortwave Radiation (Surface)

AWG Radiation Budget Application Team

Version 1.0
September 30, 2010

TABLE OF CONTENTS

1. INTRODUCTION 9
   1.1. Purpose of This Document 9
   1.2. Who Should Use This Document 10
   1.3. Inside Each Section 10
   1.4. Related Documents 10
   1.5. Revision History 11
2. OBSERVING SYSTEM OVERVIEW 11
   2.1. Products Generated 11
   2.2. Instrument Characteristics 12
3. ALGORITHM DESCRIPTION 14
   3.1. Algorithm Overview 14
   3.2. Processing Outline 14
   3.3. Algorithm Input 17
      3.3.1. Primary Sensor Data 17
      3.3.2. Ancillary Data 19
         3.3.2.1. ABI Dynamic Data 19
         3.3.2.2. Non-ABI Dynamic Data 20
         3.3.2.3. ABI-specific Static Data 20
         3.3.2.4. Non-ABI Static Data 20
         3.3.2.5. Derived Data 24
   3.4. Theoretical Description 25
      3.4.1. Physics of the Problem 25
         3.4.1.1. The physical algorithm 25
         3.4.1.2. The statistical algorithm 26
         3.4.1.3. NTB and ADM conversions 26
      3.4.2. Mathematical Description 26
         3.4.2.1. The physical algorithm 26
         3.4.2.2. The statistical algorithm 29
         3.4.2.3. NTB and ADM conversions 31
      3.4.3. Algorithm Output 31
4. Test Data Sets and Outputs 33
   4.1. Simulated/Proxy Input Data Sets 33
      4.1.1. MODIS Data 33
   4.2. Output from Simulated/Proxy Inputs Data Sets 34
      4.2.1. Precision and Accuracy Estimates 34
      4.2.2. Error Budget 35
      4.2.3. Framework Validation 37
5. Practical Considerations 37
   5.1. Numerical Computation Considerations 37
   5.2. Programming and Procedural Considerations 37
   5.3. Quality Assessment and Diagnostics 38
   5.4. Exception Handling 38
   5.5. Algorithm Validation 39
      5.5.1. Pre-Launch Phase Activities 39

5.5.2. Post-Launch Phase Activities 40
5.5.3. Correlative Data Sources 40
6. ASSUMPTIONS AND LIMITATIONS 41
6.1. Performance 41
6.2. Assumed Sensor Performance 41
6.3. Pre-Planned Product Improvements 41
6.3.1. Update NTB conversion 41
6.3.2. Update LUT 42
7. REFERENCES 42

LIST OF FIGURES

Figure 3-1. High level flowchart of the ASR algorithm illustrating the main processing sections. 15
Figure 3-2. Flowchart of the ASR physical algorithm. 16
Figure 3-3. Flowchart of the ASR statistical algorithm. 17
Figure 3-4. Global monthly mean total precipitable water for January-June. 23
Figure 3-5. Global monthly mean total precipitable water for July-December. 24
Figure 3-6. Surface albedos used in the simulation of data needed in the development of the statistical algorithm. 30
Figure 4-1. Error of ASR retrieved from MODIS proxy data as a function of ground measurements. Vertical bar represents the standard deviation of retrieval errors within each bin. 35
Figure 4-2. Errors of ABI ASR algorithm response to the perturbed input parameters. 37

LIST OF TABLES

Table 2-1. Requirements for Absorbed Shortwave Radiation at surface (ASR). 11
Table 2-2. Product qualifiers for Absorbed Shortwave Radiation at surface (ASR). 12
Table 2-3. Channel numbers and wavelengths of ABI 13
Table 3-1. ABI primary sensor data at pixel level used by both (physical and statistical) algorithms. 17
Table 3-2. ABI primary sensor input data at grid level used by both (physical and statistical) algorithms. 18
Table 3-3. ABI-derived dynamic data 19
Table 3-4. Non-ABI dynamic data used by both (physical and statistical) algorithms. 20
Table 3-5. ABI-specific static ancillary input data used in both algorithms. 20
Table 3-6. Non-ABI static ancillary input data. 21
Table 3-7. Extent of Clear-Sky Lookup Table 28
Table 3-8. Extent of Cloudy-Sky Lookup Table 28
Table 3-9. Coefficients in linear model of statistical algorithm 30
Table 3-10. Quality control flags. 31
Table 4-1. Channel mapping between ABI and MODIS. 33
Table 4-2. Ground stations used for validating retrieved ASR from MODIS proxy data 34
Table 4-3. Accuracy and precision of ASR estimation with MODIS data 35
Table 4-4. Preparation of perturbed data in each input parameters (F&PS version 2.0) 36
Table 5-1 Exceptions handled in algorithm 38

LIST OF ACRONYMS

ABI	Advanced Baseline Imager
ADM	Angular Distribution Model
ARM	Atmospheric Radiation Measurement project
ASR	Absorbed Shortwave Radiation at surface
ASTER	Advanced Space Thermal Emission and Reflection Radiometer
ATBD	Algorithm Theoretical Basis Document
AVHRR	Advanced Very High Resolution Radiometer
AWG	Algorithms Working Group
CAVE	CERES/ARM Validation Experiment
CERES	Clouds and the Earth's Radiant Energy System
CMDL	Climate Monitoring and Diagnostics Laboratory
DSR	Downward Shortwave Radiation at Surface
ESRL/GMD	Earth System Research Laboratory/Global Monitoring Division
F&PS	Functional and Performance Specification
GOES	Geostationary Operational Environmental Satellite
GVI	Global Vegetation Index
JPSS	Joint Polar Satellite System
LaRC	Langley Research Center
LUT	Lookup Table
MODIS	Moderate Resolution Imaging Spectroradiometer
MODTRAN	Moderate Resolution Radiative Transfer Models
MRD	Mission Requirements Document
NASA	National Aeronautics and Space Administration
NESDIS	National Environmental Satellite, Data, and Information Service
NOAA	National Oceanic and Atmospheric Administration
NPOESS	National Polar-orbiting Operational Environmental Satellite System
NTB	Narrow-to-Broadband
OAR	Office of Oceanic and Atmospheric Research
RAZ	Relative Azimuth Angle
PSGS	Perot Systems Government Services
RTM	Radiative Transfer Model
SARB	Surface and Atmospheric Radiation Budget
SEVIRI	Spinning Enhanced Visible and Infra-red Imager
SRB	Shortwave Radiation Budget
STAR	Center for Satellite Applications and Research
SURFRAD	Surface Radiation Budget Network
SW	Shortwave
SZA	Solar Zenith Angle
TIGR	TIROS Initial Guess Retrieval
TOA	Top of Atmosphere
UMD	University of Maryland

USGS	United States Geological Survey
VZA	Viewing Zenith Angle

ABSTRACT

This document describes the physical and mathematical basis of the algorithm developed for retrieving the absorbed shortwave radiation at the surface from the radiance measurements of, and atmosphere products derived from the Advanced Baseline Imager onboard the geostationary satellite GOES-R. When data needed to describe the composition of the atmosphere are available from preceding ABI retrievals and/or ancillary sources the algorithm retrieves the radiative fluxes in a forward scheme using a look-up-table representation of the radiative transfer. When the needed ABI products are not available the algorithm estimates the surface absorbed flux from a predefined relationship between top-of-atmosphere broadband albedo and surface absorbed flux parameterized in terms of the solar zenith angle and water vapor amount. Both algorithms require broadband top-of-atmosphere albedo derived from the narrowband ABI radiances by appropriate spectral and angular transformations.

The algorithm is tested with proxy data from MODIS. Performance is evaluated by comparison with ground measurements of absorbed shortwave radiation at the surface from the SURFRAD, ARM, and CMDL networks. The accuracy and precision are found to be functions of the measured quantity. Overall, the fluxes are estimated by an accuracy of better than about 4%. Quality of the retrieval is indicated by flags that are set according to the quality of input, retrieval conditions, and expected range of output.

Validations in the pre-launch and post-launch phases use similar methods and tools with MODIS as proxy data and CERES, SURFRAD, BSRN and the future SEBN as sources of reference data.

Update of the LUT by using atmospheric properties consistent with those used by other AWG Application Teams, and a common radiative transfer model (if possible), stratification of narrow-to-broadband conversions according to elevation dependence are planned.

1. INTRODUCTION

The balance between the solar input and the thermal output is known as the Earth's Radiation Budget. The shortwave radiation absorbed at the surface (ASR) associated with the solar input is an important component of this budget. The ASR is defined as the difference between downward and upward solar radiation at the surface. It is affected by the nature of the Earth's surface and its atmosphere, particularly clouds. The ASR drives the processes of evaporation, air and soil heating, as well as other, smaller energy-consuming processes such as photosynthesis. The ASR influences, therefore, atmospheric circulations, as well as surface climate, and is used in numerical weather simulations and surface modeling.

The ASR can be directly calculated from knowing the downward and upward shortwave radiation at the surface (DSR). The upward shortwave radiation at the surface is, however, not a required GOES-R ABI product, and as such it is considered unavailable. In principle, the upward flux could be calculated from the DSR and the surface albedo. However, analysis of the surface albedo estimated from the imagers onboard the current GOES in the operational GOES Surface and Insolation Products system indicates large uncertainties (Laszlo et al.,2004). (It is noted that a GOES-R Option 2 surface albedo product currently being developed by the AWG Land Application Team may have an improved quality over that from GSIP. However, this could not be confirmed at this time.)

An alternative way, which does not require explicit knowledge of the surface albedo, for deriving the ASR is to use a direct relationship between TOA and surface net fluxes. Ramanathan (1986) found a simple linear relationship between the net solar flux at the TOA and that at the surface based on a climate model. Laszlo and Pinker (1994) also showed, based on radiative transfer arguments, that surface and TOA fractional absorptions are very linearly correlated. Linear regression was used to link ASR and satellite observations in many studies (e.g., (Cess et al.,1991; Li et al.,1993; Schmetz,1993). The satellite observations used in these studies varied. For example, broadband satellite data from the Earth Radiation Budget Experiment (ERBE) data were used by (Cess et al.,1991; Cess and Vulis,1989; Li et al.,1993; Masuda et al.,1995), while narrowband radiances at coarse spatial resolution, such as those in the International Satellite Cloud Climatology Project (ISCCP) data, were used by others (Laszlo and Pinker,2002; Pinker and Laszlo,1992; Rossow and Zhang,1995; Zhang et al.,2004), Higher spatial resolution narrowband radiances, such as those from the Moderate Resolution Imaging Spectroradiameter (MODIS) were also employed (Kim and Liang,2010; Tang et al.,2006). The basic principle of the methods used is the fact that atmospheric absorption remains relatively constant when compared to the variability of the radiation absorbed at the surface or the TOA (Pinker et al.,1995).

1.1. Purpose of This Document

This Algorithm Theoretical Basis Document (ATBD) provides a description of the physical basis and the algorithm for the retrieval of absorbed shortwave (SW: 0.2-4.0 μm) radiation at the

surface (ASR) from radiances measured by and atmospheric products derived from the Advanced Baseline Imager (ABI) flown on the GOES-R series of NOAA geostationary environmental satellites. It describes a hybrid algorithm which combines a physical and a statistical algorithm. The document also provides details on the evaluation of algorithm performance during the development phase.

1.2. Who Should Use This Document

The intended users of this document are those interested in understanding the physical basis of the absorbed shortwave radiation algorithm and how the evaluation of the algorithm and its products were performed. This document also provides information useful to anyone maintaining or modifying the original algorithm.

1.3. Inside Each Section

This document is broken down into the following main sections.

- **System Overview**: Provides relevant details of the ABI and provides a brief description of the products generated by the algorithm.

- **Algorithm Description**: Provides all the detailed description of the algorithm including its physical basis, its input and its output.

- **Test Data Sets and Output**: Provides a description of the test data set used to characterize the performance of the algorithm and quality of the data products.

- **Practical Considerations**: Provides an overview of the issues involving numerical computation, programming and procedures, quality assessment and diagnostics and exception handling.

- **Assumptions and Limitations**: Provides an overview of the current limitations of the approach and gives the plan for overcoming these limitations with further algorithm development.

1.4. Related Documents

This document relates to the references given throughout and to the following documents:

GOES-R Mission Requirements Document (MRD)
GOES-R Ground Segment Functional and Performance Specification Document (F&PS)

GOES-R Advanced Baseline Imager (ABI) Algorithm Theoretical Basis Document for Downward Shortwave Radiation (Surface), and Reflected Shortwave Radiation (TOA), Ver. 3

GOSE-R ABI *Absorbed Shortwave Radiation: Surface* Algorithm and Test Implementation Plan (ATIP) Document

1.5.Revision History

This is the first version (Version 1.0) of this document for 80% maturity delivery. This document describes Version 3 of the ASR algorithm. It was written by Dr. Istvan Laszlo (NOAA/STAR), Dr. H.-Y. Kim (IMSG) and Dr. Hongqing Liu (Dell/QSS) with inputs from Dr. Ellsworth G. Dutton of NOAA/OAR on the ground data used in the evaluation of the algorithm. Sections 3.4.1.3 and 3.4.2.3 are based on inputs from Prof. Rachel T. Pinker, Ms. Xiaolei Niu, and Dr. Margaret Wonsick (all UMD/AOSC).

2. OBSERVING SYSTEM OVERVIEW

This section describes the products generated by the algorithm and the requirements it places on the sensor. It also provides an overview of the retrieval strategy, the algorithm, and the input needed for the ASR algorithm.

2.1.Products Generated

The ABI ASR algorithm generates the Absorbed Shortwave Radiation at Surface (ASR) products at mesoscale.

ASR, defined as the difference between downward and upward solar radiation at the surface , regulates the redistribution of energy at the surface/atmosphere interface (Pinker and Tarpley,1988). Over land, ASR controls the input of latent and sensible heat flux into the atmosphere; over ocean, it controls the oceanic heating which is associated with long term weather and climate variability. Information about radiative fluxes at the surface is essential for climate related studies on all time and spatial scales (Pinker et al.,1985). The GOES-R based ASR due to its resolution of the diurnal cycle can be complementary to other ASR products at lower temporal resolution (for example, CERES; (Wielicki et al.,1996). ASR is given in the units of Wm^{-2}.

Tables 2-1 and 2-2 show the current F&PS requirements and product qualifiers (version 2.1) for the ABI ASR products.

Table 2-1. Requirements for Absorbed Shortwave Radiation at surface (ASR).

Name	User & Priority	Geographic Coverage (G, H, C, M)	Vertical Resolution	Horizontal Resolution	Mapping Accuracy	Measurement Range	Measurement Accuracy	Refresh Rate/Coverage Time Option (Mode 3)	Refresh Rate Option (Mode 4)	Vendor Allocated Ground Latency	Product Measurement Precision
Absorbed Solar Insolation: surface	GOES-R	M	N/A	5 km	1 km	0 – 1200 Wm^{-2}	90 Wm^{-2} at low value (100 Wm^{-2}); 45 Wm^{-2} at mid value (400 Wm^{-2}); 55 Wm^{-2} at high value (800 Wm^{-2})	60 min	N/A	3236 sec	75 Wm^{-2} for low and high values (100 and 800 Wm^{-2}) and 95 Wm^{-2} for mid values (400 Wm^{-2})

M=mesoscale

Table 2-2. Product qualifiers for Absorbed Shortwave Radiation at surface (ASR).

Name	User & Priority	Geographic Coverage (G, H, C, M)	Temporal Coverage Qualifiers	Product Extent Qualifier	Cloud Cover Conditions Qualifier	Product Statistics Qualifier
Absorbed Solar Insolation: surface	GOES-R	M	Day	Quantitative out to at least 70 degrees LZA and qualitative beyond	N/A	Over specified geographic area

LZA=local zenith angle

2.2. Instrument Characteristics

The Advanced Baseline Imager (ABI) on GOES-R will have a total of 16 spectral bands in the visible, near-infrared and infrared spectral regions. The ABI spatial resolution will be 2.0 km for the 1.38-µm, 2.25-µm and ten infrared (IR) spectral bands, and 0.5 km for the 0.64-µm visible band. Spatial resolution of the other bands will be 1.0 km. Table 2-3 lists these and the spectral characteristics of the instrument. ABI will have an on-board calibration of the reflected solar channels and expected to provide an absolute radiometric calibration accuracy of 5.0%, relative (one-sigma) calibration deviations (short-term repeatability) of 0.2%, calibrated radiances that correct for instrument degradation drift in radiance to 0.5% of the radiance. (Additional observations of lunar or stellar sources may be employed by NOAA operationally to attempt to improve long-term radiometric stability of the on-board calibration methodology over the ABI lifetime.) Details on the instrument design, calibration, and additional information on its characteristics are provided elsewhere, and not included in this ATBD.

The ASR algorithm will use observations in selected channels (see Table 2-3). The selected channel observations are used to obtain the TOA broadband albedo from the ABI narrowband reflectances. The performance of the algorithm is therefore sensitive to any imagery artifacts or instrument noise.

Table 2-3. Channel numbers and wavelengths of ABI

Channel ID	***Wavelength Microns***	***Hor. Res.***	***Upper and lower 50% response points (in microns)***	***Noise @ Ref.***	***Max. Level***	***Used in ASR***
1	0.47	1km	0.45±0.01 - 0.49±0.01	300/1	100 %	✓
2	0.64	0.5km	0.59±0.01 - 0.69±0.01	300/1	100 %	✓
3	0.865	1km	0.8455±0.01 - 0.8845±0.01	300/1	100 %	✓
4	1.378	2km	1.3705±0.005 - 1.3855±0.005	300/1	100 %	✓
5	1.61	1km	1.58±0.01 - 1.64±0.01	300/1	100 %	✓
6	2.25	2km	2.225±0.01 - 2.275±0.01	300/1	100 %	✓
7	3.90	2km	3.80±0.05 - 4.00±0.05	0.1 K	400 K	
8	6.185	2km	5.77±0.03 - 6.6±0.03	0.1 K	300 K	
9	6.95	2km	6.75±0.03 - 7.15±0.03	0.1 K	300 K	
10	7.34	2km	7.24±0.02 - 7.44±0.02	0.1 K	320 K	
11	8.5	2km	8.3±0.03 - 8.7±0.03	0.1 K	330 K	
12	9.61	2km	9.42±0.02 - 9.8±0.03	0.1 K	300 K	
13	10.35	2km	10.1±0.1 - 10.6±0.1	0.1 K	330 K	
14	11.2	2km	10.8±0.1 - 11.6±0.1	0.1 K	330 K	
15	12.3	2km	11.8±0.1 - 12.8±0.1	0.1 K	330 K	
16	13.3	2km	13.0±0.06 - 13.6±0.06	0.3 K	305 K	

3. ALGORITHM DESCRIPTION

This section describes the ABI ASR algorithm at the current level of maturity.

3.1. Algorithm Overview

The ABI ASR algorithm is developed as a hybrid algorithm based on the NESDIS/STAR ASR physical algorithm (Laszlo and Pinker,1994, 2002) and on the NESDIS/STAR ASR statistical algorithm. The primary algorithm is the physical algorithm, which mostly uses ABI products (e.g., cloud cover, optical depth, size and phase, and aerosol optical depth and type) to estimate the ASR in a forward calculation. When these ABI products are not available the algorithm switches to the statistical algorithm which only needs precipitable water amount in retrieval of ASR. Both algorithms need the SW broadband TOA albedo estimated from the narrowband ABI reflectances by spectral NTB transformations and angular corrections.

3.2. Processing Outline

The overall processing of the ASR algorithm is summarized in Figure 3-1. The current ASR algorithm is implemented at the grid level consistent with the product horizontal resolution specified in the F&PS. Within each grid, TOA broadband albedo retrieval is carried out for each of three primary scene types (clear, water cloud, and ice cloud). The physical algorithm calculates the clear-sky and cloudy-sky fluxes separately, and arrives to the all-sky flux by weighting the scene-based fluxes by their scene fraction. The statistical algorithm uses the scene fraction weighted TOA broadband albedo to yield the scene-averaged ASR. Algorithm inputs are prepared by collecting and averaging ancillary and ABI sensor data within the spatial grids predefined for outputs. Up to three scene types (clear sky, water cloud and ice cloud) are determined within each grid and the corresponding ABI channel reflectances are averaged separately.

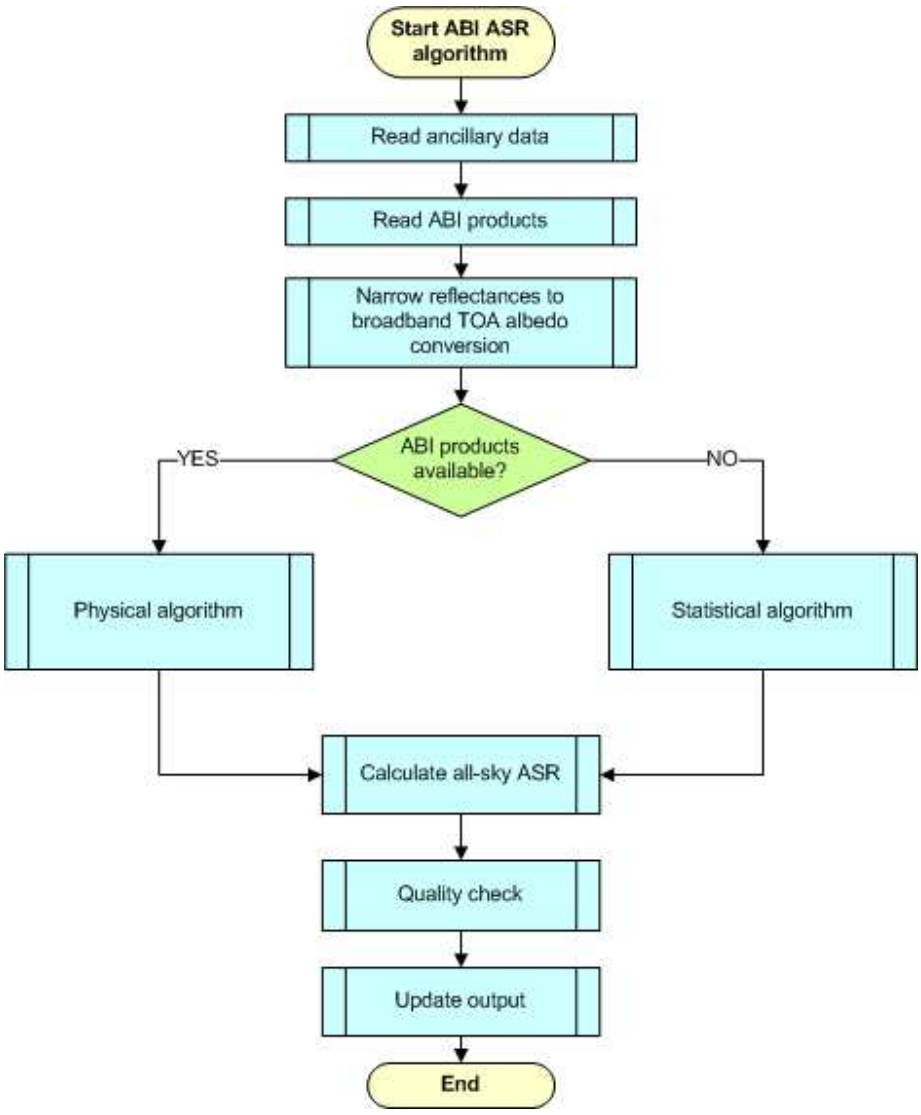

Figure 3-1. High level flowchart of the ASR algorithm illustrating the main processing sections.

The retrieval process uses two algorithms and the selection of algorithm is based on the availability of ABI Level 2 retrieval products on a grid basis.

- The physical algorithm is applied when the required preceding ABI atmosphere products are available. ASR is calculated directly from the inputs of atmospheric composition. The atmospheric transmittances and reflectances (optical functions) needed for this are pre-calculated for discrete values of these inputs, and are stored in lookup tables. The ABI product inputs are used to calculate these optical functions for the actual inputs by interpolating the atmospheric optical functions in the lookup tables. Figure 3-2 presents a schematic illustration of the physical algorithm retrieval.

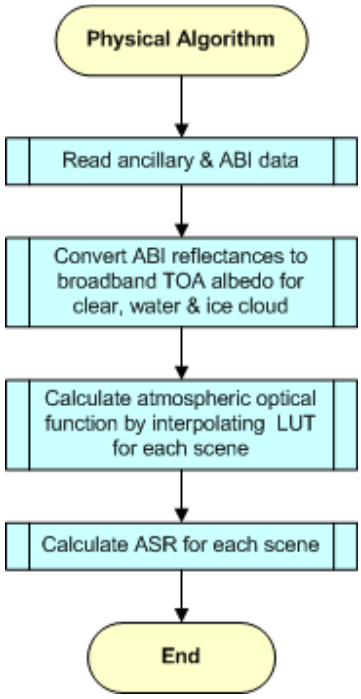

Figure 3-2. Flowchart of the ASR physical algorithm.

- The statistical algorithm is applied when the absence of a required ABI product prohibits the retrieval from the physical algorithm. The approach requires the solar zenith angle and the total column amount of precipitable water to determine the slope and offset for estimating ASR from the scene averaged broadband TOA albedo. A schematic illustration of the statistical algorithm is presented in Figure 3-3.

The selection of the retrieval algorithm is determined at the grid (not scene) level, meaning a grid has ASR retrieved solely from either the physical or the statistical algorithm (that is algorithms are not “mixed” within a single grid). Quality flags appended to the output indicate the algorithm used for a given grid.

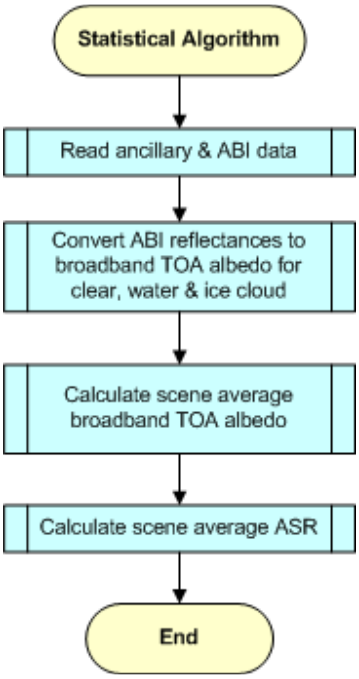

Figure 3-3. Flowchart of the ASR statistical algorithm.

3.3. Algorithm Input

This section describes the attributes of all input data used by the algorithm, including primary sensor data, ancillary data, radiative transfer models, and look-up tables.

3.3.1. Primary Sensor Data

Table 3-1 lists the primary sensor data (data directly available from ABI) used by the ASR algorithm, including calibrated ABI Level 1B reflectances, geolocation information, and ABI sensor quality flags. All inputs are pixel level data with (xsize, ysize) denoting the two-dimensional (longitude-latitude) input size.

Table 3-1. ABI primary sensor data at pixel level used by both (physical and statistical) algorithms.

Name	Type	Description	Dimension
Ch1 reflectance	Input	Calibrated ABI level 1b reflectance at channel 1 - 0.47µm	pixel (xsize, ysize)
Ch2 reflectance	Input	Calibrated ABI level 1b reflectance at channel 2 - 0.64µm	pixel (xsize, ysize)
Ch3 reflectance	Input	Calibrated ABI level 1b reflectance at channel 3 - 0.86µm	pixel (xsize, ysize)
Ch5 reflectance	Input	Calibrated ABI level 1b reflectance at	pixel (xsize, ysize)

		channel 5 - 1.61μm	
Ch6 reflectance	Input	Calibrated ABI level 1b reflectance at channel 6 - 2.26μm	pixel (xsize, ysize)
Latitude	Input	Center latitude	pixel (xsize, ysize)
Longitude	Input	Center longitude	pixel (xsize, ysize)
Solar geometry	Input	ABI solar zenith and azimuth angles	pixel (xsize, ysize)
View geometry	Input	ABI view zenith and azimuth angles	pixel (xsize, ysize)
QC flags	Input	ABI quality control flags with level 1b data	pixel (xsize, ysize)

Both algorithms need the reflectance data to establish the connection between reflection at TOA and absorption at surface. To be consistent with the horizontal resolution of the radiation products, pixel level sensor data are averaged within the required spatial grid (5 km). The averaging of reflectances is done separately for the three main scene types (clear sky, water cloud and ice cloud) based on the ABI cloud mask and retrieved cloud phase. In this version, simple arithmetic averages of the reflectances are calculated. The grid level sensor inputs are summarized in Table 3-2.

Table 3-2. ABI primary sensor input data at grid level used by both (physical and statistical) algorithms.

Name		Type	Description	Dimension
Clear-sky reflectance	Ch1	Input	Mean calibrated ABI level 1b reflectance at channel 1 for clear-sky pixels	grid (xsize, ysize)
	Ch2	Input	Mean calibrated ABI level 1b reflectance at channel 2 for clear-sky pixels	grid (xsize, ysize)
	Ch3	Input	Mean calibrated ABI level 1b reflectance at channel 3 for clear-sky pixels	grid (xsize, ysize)
	Ch5	Input	Mean calibrated ABI level 1b reflectance at channel 5 for clear-sky pixels	grid (xsize, ysize)
	Ch6	Input	Mean calibrated ABI level 1b reflectance at channel 4 for clear-sky pixels	grid (xsize, ysize)
Water-cloud reflectance	Ch1	Input	Mean calibrated ABI level 1b reflectance at channel 1 for water-cloud pixels	grid (xsize, ysize)
	Ch2	Input	Mean calibrated ABI level 1b reflectance at channel 2 for water-cloud pixels	grid (xsize, ysize)
	Ch3	Input	Mean calibrated ABI level 1b reflectance at channel 3 for water-cloud pixels	grid (xsize, ysize)
	Ch5	Input	Mean calibrated ABI level 1b reflectance at channel 5 for water-cloud pixels	grid (xsize, ysize)
	Ch6	Input	Mean calibrated ABI level 1b reflectance at channel 4 for water-cloud pixels	grid (xsize, ysize)
Ice-cloud reflectance	Ch1	Input	Mean calibrated ABI level 1b reflectance at channel 1 for ice-cloud pixels	grid (xsize, ysize)
	Ch2	Input	Mean calibrated ABI level 1b reflectance at channel 2 for ice-cloud pixels	grid (xsize, ysize)

	Ch3	Input	Mean calibrated ABI level 1b reflectance at channel 3 for ice-cloud pixels	grid (xsize, ysize)
	Ch5	Input	Mean calibrated ABI level 1b reflectance at channel 5 for ice-cloud pixels	grid (xsize, ysize)
	Ch6	Input	Mean calibrated ABI level 1b reflectance at channel 4 for ice-cloud pixels	grid (xsize, ysize)
Latitude		Input	Center latitude	grid (xsize, ysize)
Longitude		Input	Center longitude	grid (xsize, ysize)
Solar geometry		Input	ABI solar zenith and azimuth angles	grid (xsize, ysize)
View geometry		Input	ABI view zenith and azimuth angles	grid (xsize, ysize)
QC flags		Input	ABI quality control flags with level 1b data	grid (xsize, ysize)

3.3.2. Ancillary Data

The algorithm requires four types of ancillary data:

- ABI-derived dynamic data (Table 3-3)
- Non-ABI dynamic (Table 3-4)
- ABI-specific static data (Table 3-5)
- Non-ABI static data (Table 3-6)

3.3.2.1. ABI Dynamic Data

Table 3-3 lists the input data expected to come from ABI retrievals.

Table 3-3. ABI-derived dynamic data

Name	Type	Description	Dimension
Cloud mask [p]	Input	ABI level 2 cloud mask	grid (xsize, ysize)
Cloud phase [p]	Input	ABI level 2 cloud top phase data	grid (xsize, ysize)
Cloud optical depth [p]	Input	ABI level 2 cloud optical depth data	grid (xsize, ysize)
Cloud particle size [p]	Input	ABI level 2 cloud particle size	grid (xsize, ysize)
Cloud top height [p]	Input	ABI level 2 cloud top height	grid (xsize, ysize)
Aerosol optical depth [p]	Input	ABI level 2 aerosol optical depth data	grid (xsize, ysize)
Aerosol type [p]	Input	ABI level 2 aerosol type data	grid (xsize, ysize)
Snow/Ice mask [b]	Input	ABI level 2 Snow cover data	grid (xsize, ysize)
Total precipitable water [b]	Input	ABI level 2 total precipitable water	grid (xsize, ysize)
Ozone [p]	Input	ABI level 2 ozone data	grid (xsize, ysize)

* [p]: used by physical algorithm only; [b]: used by both paths

3.3.2.2. Non-ABI Dynamic Data

When the ABI snow/ice mask (Fractional Snow Cover (FSC), or Snow Cover) is not available, data from the Interactive Multisensor Snow and Ice Mapping System (IMS) are used.

Table 3-4. Non-ABI dynamic data used by both (physical and statistical) algorithms.

Name	Type	Description	Dimension
Model snow/ice mask	input	Ice Mapping System (IMS) data	grid (xsize, ysize)

3.3.2.3. ABI-specific Static Data

The ABI static data include the conversion factors used to estimate the SW broadband reflectance from the ABI narrow-band reflectances in the five SW channels 1, 2, 3, 5, and 6 (see Section 3.4.1.3). To capture the spectral variation of TOA radiation under various conditions, conversion coefficients are developed for different sun-sensor geometry and surface types under clear condition. Ten solar zenith angle bins are adopted with central values being 12.9º, 30.8º, 41.2º, 48.3º, 56.5º, 63.2º, 69.5º, 75.5º, 81.4º and 87.2º. These angles are selected such that their cosine values are uniformly distributed between 0.05 and 0.95 with a step of 0.1. Twelve International Geosphere-Biosphere Programme (IGBP) surface types are adopted under clear conditions including water; needleleaf forest; broadleaf forest; mixed forest; woody savannas; savannas; closed shrubs; open shrubs; grasslands; croplands; bare ground; and snow/ice. For cloudy cases, nine cloud types are considered: cumulus, altostratus, stratus, stratocumulus, nimbostratus, cirrus over ocean, cirrus over shrub, cirrus over desert, and cirrus over snow/ice. The number of coefficients needed (Ncoef in Table 3-5) is a function of the instrument; for ABI the currently expected value is 6 for each scene type.

Table 3-5. ABI-specific static ancillary input data used in both algorithms.

Name	Type	Description	Dimension
Narrow-to-Broadband Conversion Factor	Input	Coefficients for converting satellite narrowband reflectance to broadband TOA albedo under **clear** condition	(6,10,12) (Ncoef, Nsza, Nsfctype)
		Coefficients for converting satellite narrowband reflectance to broadband TOA albedo under **cloudy** condition	(6,9) (Ncoef, NcldType

3.3.2.4. Non-ABI Static Data

One of the major non-ABI Static data is the spectral lookup tables (LUT) of atmospheric reflection, direct/diffuse transmission and spherical reflection/transmission used by the physical

algorithm. The LUT is identical to that used in the baseline algorithm for the retrieval of the Shortwave Radiation at surface (DSR) and Shortwave Radiation at TOA (RSR). Detailed information of the LUT is presented in section 3.4.2.1 of this document. Surface elevation data is also needed by the physical algorithm, and is currently taken from the Global 30 Arc-Second Elevation Data Set (GTOPO30) of US Geological Survey (USGS) global topographic data digital elevation model. High resolution data will be averaged to the spatial grid predefined for ASR. Relevant details of GTOPO30 data are available from http://eros.usgs.gov/products/elevation/gtopo30.php.

There are multiple ancillary data used in both (physical and statistical) algorithms:

- The International Geosphere-Biosphere Programme (IGBP) surface types are used to provide background information for the spectral surface albedo and TOA albedo conversion. Binary surface-type map at 1/6-degree resolution is taken from the CERES/SARB surface properties website (http://www-surf.larc.nasa.gov/surf/pages/data-page.html). It is anticipated that a low spatial resolution map of surface type will be prepared to be compatible with product resolution.
- Land/Sea mask is used to identify the coastal region where retrievals might be of degraded quality.
- Monthly climatology of total precipitable water is derived from 30 years of NCEP/DOE Reanalysis II monthly mean data (Jan. 1979 – Dec. 2008) with 2.5 º × 2.5 º spatial resolution (Figure 3-4 and Figure 3-5). It is used when the ABI total precipitable water product is not available.
- The NTB conversion implemented in Version 3 of the algorithm accounts for the solar angle only. (Conversion coefficients that also depend on viewing angle and azimuth angle were developed and tested. These tests, however, indicated that the only-solar-angle-dependent conversions had superior performance when compared to TOA albedo observations. Therefore in Version 3 of the algorithm the conversion implemented depends only on the solar angle.) TOA broadband reflectance-to-albedo conversion adopts the CERES TRMM Angular Distribution Models (ADM) for clear and cloudy sky over land and ocean (Loeb et al., 2003), and the CERES Terra ADMs over snow/ice (Kato and Loeb, 2005).

It should be noted that with further algorithm development the ancillary data used may be subject to change.

Table 3-6. Non-ABI static ancillary input data.

Name	Type	Description	Dimension
Surface Height [p]	Input	US Geological Survey (USGS) global topographic data digital elevation model	(43200,21600) (Nlon, Nlat)
Surface Type [b]	Input	International Geosphere-Biosphere Programme (IGBP) surface types	(2160,1080) (Nlon, Nlat)
Total Precipitable Water	Input	NCEP/DOE Reanalysis II monthly mean data	(144,73,12) (Nlon,Nlat)

Climatology [b]			
Land/Sea Mask [b]	Input	Global land/water/coast mask	1km
TOA Angular Distribution Model [b]	Input	CERES ADM for clear land	(10, 9, 9, 4) (NrelAzi, NsatZen, NsolZen, NsfcType)
		CERES ADM for clear ocean	(10, 9, 9, 4) (NrelAzi, NsatZen, NsolZen, NwndSpd)
		CERES ADM for cloudy land	(10, 9, 9, 6, 4, 2) (NrelAzi, NsatZen, NsolZen, NcldOd, NsfcType, NcldPhase)
		CERES ADM for cloudy ocean	(10, 9, 9, 14, 2) (NrelAzi, NsatZen, NsolZen, NcldOd, NcldPhase)
		CERES ADM for permanent snow	(10, 9, 45, 3, 2) (NrelAzi, NsatZen, NsolZen, NcldOd, NsfcType)
		CERES ADM for fresh snow	(10, 9, 18, 3, 2) (NrelAzi, NsatZen, NsolZen, NcldOd, NsfcType)
		CERES ADM for sea ice	
		CERES ADM for fractional fresh snow	(10, 9, 18, 7) (NrelAzi, NsatZen, NsolZen, NsnowIceFrac)
		CERES ADM for fractional sea ice	
Lookup Table [b]	Input	Atmosphere reflection	(18,15,7,3,5,7,4) for clear sky (Nband, Nsza, Ntpw, No3, NsfcElv, Naod, Nssa) (18,15,7,3,5,12,4,5,2) for water/ice cloud (Nband, Nsza, Ntpw, No3, NsfcElv, Ncod, NcldRad, NcldHgt, NcldPhase)
		Atmosphere direct transmission	
		Atmosphere diffuse transmision	
		Atmosphere spherical albedo	
		Atmosphere spherical transmission	

* [p]: used by physical algorithm only; [b]: used by both algorithms

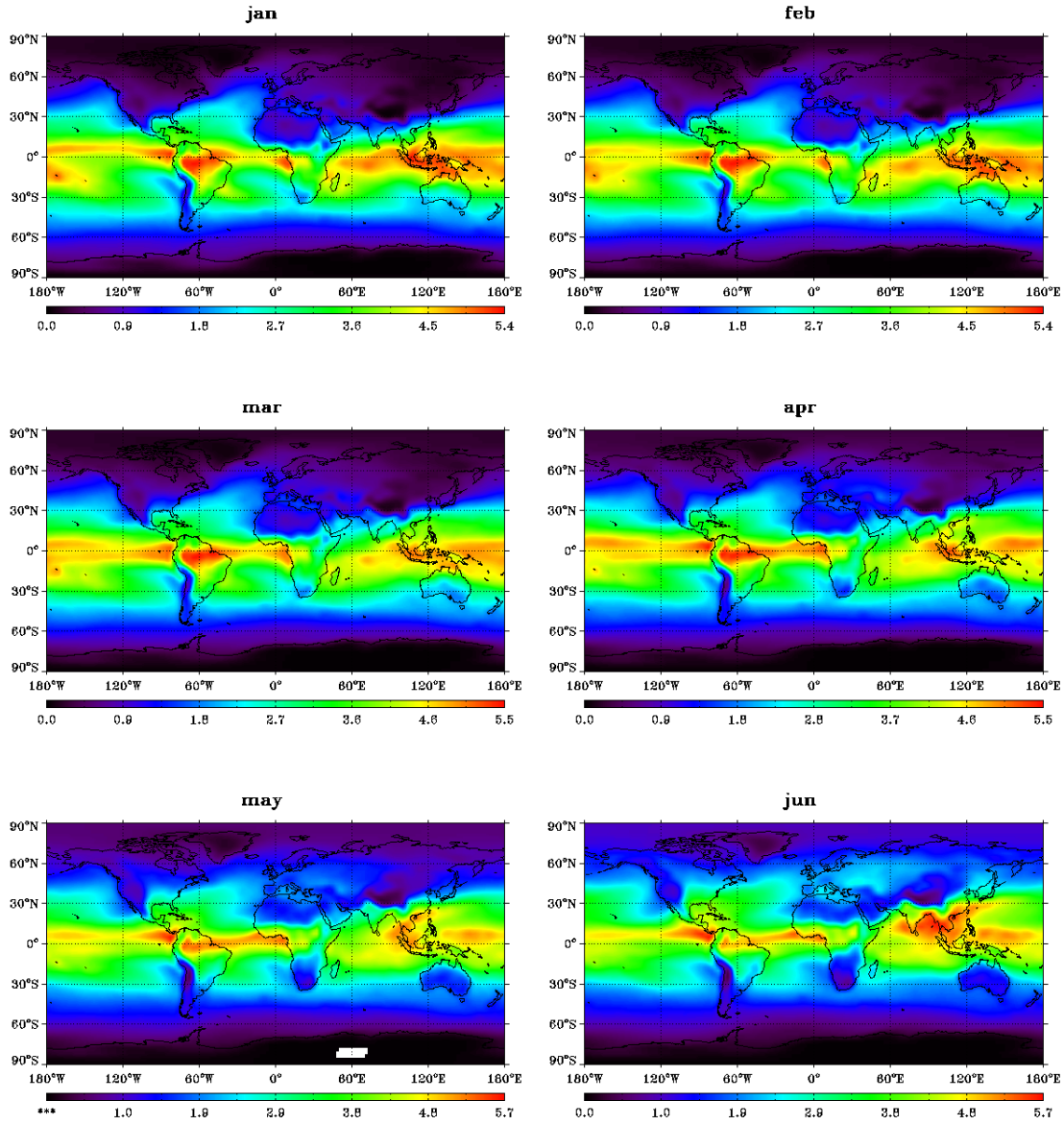

Figure 3-4. Global monthly mean total precipitable water for January-June.

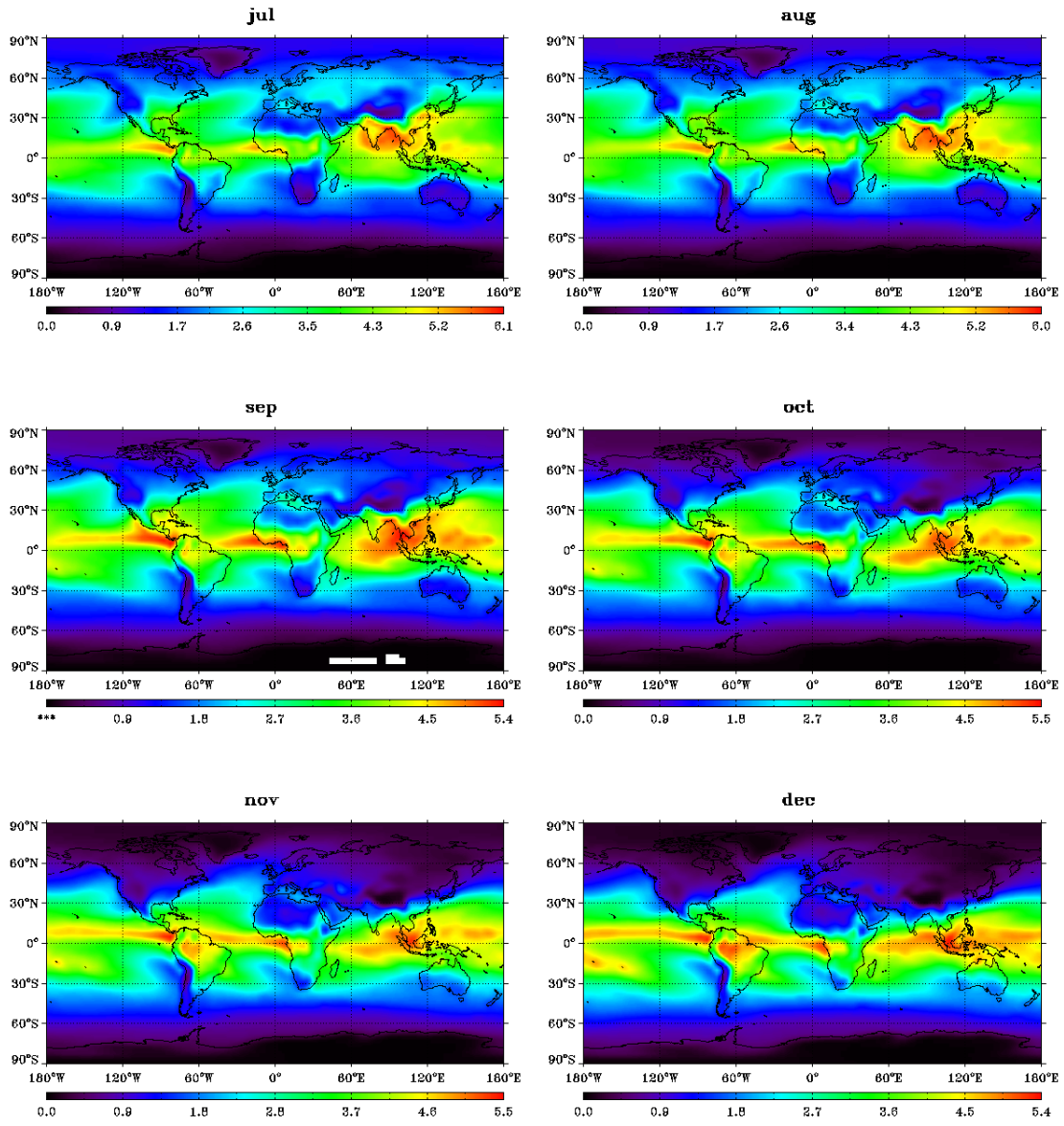

Figure 3-5. Global monthly mean total precipitable water for July-December.

3.3.2.5. Derived Data

N/A

3.4. Theoretical Description

This section describes the physics, radiative transfer, and associated phenomenology key to the retrieval. Description of the mathematics used by the retrieval, including all simplifications, approximations, and numerical methods are also presented, as well as description of the output of the algorithm as encoded in the data product.

3.4.1. Physics of the Problem

The amount of radiation absorbed by a medium is measured by the difference between the radiative energy entering and exiting the medium, and is referred to as the net flux. The net flux at TOA is usually obtained from satellite data, and is considered measured even though in reality only the upward component of it is observed. The net flux at the surface is measured directly only at a limited number of sites; on global scale it is usually derived from satellite measurements using a relationship between TOA and surface values. Model simulations and measurements indicate a near-linear relationship between surface solar absorption and surface-atmosphere solar absorption (Cess and Vulis,1989; Ramanathan,1986). This direct relationship can be used to estimate ASR when the absorbed SW radiation at TOA is known. The relationship is either estimated empirically (e.g., (Cess and Vulis,1989; Li et al.,1993)) or obtained from modeling (Laszlo and Pinker,2002).

3.4.1.1. The physical algorithm

The physical algorithm uses a relationship between surface and TOA solar absorption that is directly established from reflectance (R) and transmittance (T) of the surface-atmosphere as calculated from a radiative transfer model (RTM). The reflectances and transmittances needed are stored in a lookup table. In Version 3 of the ABI algorithm the radiative transfer model used to generate the lookup table is the NASA Langley modified Fu-Liou RTM (Fu and Liou, 1993) with column amounts of water vapor and ozone, aerosol and cloud optical depth, and cloud fraction as primary inputs. In principle any other accurate RTM that is capable of calculating radiative fluxes in the entire shortwave spectrum could be used to generate the lookup table. To this end, it is noted that broadband transmission and TOA albedo is highly dependent on cloud cover and optical properties. Any uncertainty in the retrieval of cloud and aerosol properties will overwhelm the errors raised from radiative transfer calculations.

The complexity of the lookup table increases with the number of input variables. To make the LUT manageable and be as accurate as possible, tables of atmospheric reflectivity, direct and diffuse transmissivity, and spherical reflectivity and transmissivity at 18 spectral bands were generated corresponding to the scenes of clear-sky, water cloud and ice cloud.

Because the physical algorithm uses ABI derived parameters as inputs the fluxes derived are expected to be consistent with these parameters. However, in order to achieve closure at TOA and surface simultaneously with true net fluxes at these boundaries, these parameters must be consistent with each other and with the true net flux at TOA. In reality these parameters have errors and full simultaneous closure cannot be achieved. Forcing a closure at TOA could easily increase the errors at the surface. This is the primary limitation of the physical algorithm. This is

coupled with the unavoidable error in the estimated TOA absorption, which may further increase the error in the surface absorption depending on the sign of the error in the TOA value.

3.4.1.2. The statistical algorithm

The statistical algorithm uses a relationship between surface and TOA solar absorption that was established by a linear regression model. Data used in the regression are calculated by the modified Fu-Liou code (the same RTM used to generate the lookup table for the physical algorithm). This relationship is parameterized a function of the solar zenith angle and the total column amount of precipitable water following Li et al. (1993) who pointed out the explicit role of solar zenith angle and water vapor in that relationship.

Both the physical and the statistical algorithms require an estimate of the TOA broadband albedo. The method used for getting this albedo is discussed in the next section.

3.4.1.3. NTB and ADM conversions

Both the physical and statistical algorithms require the knowledge of the SW (broadband) TOA albedo. This is accomplished by a module developed at the University of Maryland (UMD) that estimates the SW TOA albedo from the narrowband ABI reflectances. Basically the module performs two steps:

1. Transformation of narrowband reflectances into broadband ones using spectral transformations (narrow-to-broadband conversion; NTB);
2. Transformation of broadband reflectances into broadband albedo by applying Angular Distribution Models (ADMs).

The details are provided in the "GOES-R Advanced Baseline Imager (ABI) Algorithm Theoretical Basis Document for Downward Shortwave Radiation (Surface), and Reflected Shortwave Radiation (TOA), Ver. 3", and not repeated here.

3.4.2. Mathematical Description

The physical and statistical algorithms adopt different schemes to calculate ASR. Their mathematical details are introduced in the following sections.

3.4.2.1. The physical algorithm

Based on the conservation of radiative energy in the surface-atmosphere system one can write:

$$n_{SRF} = n_{TOA} - n_{ATM} \qquad (1)$$

$$\text{where } n = \frac{\text{absorbed energy}}{\text{incident energy}}$$

and the subscripts SRF, TOA, and ATM refer to the fraction of solar energy absorbed at the surface, at the TOA (by the surface-atmosphere system), and by the atmosphere, respectively. The incident energy is $S_0 \cos(\theta_0)\frac{d_0^2}{d^2}$, where S_0 is the solar constant, θ_0 is the solar zenith angle, d and d_0 are the actual and mean Sun-Earth distances, respectively.

The difference $n_{TOA} - n_{ATM}$ can be expressed as a function of atmospheric composition and n_{TOA} (Laszlo and Pinker,1994, 2002). Using the adding equations of the radiative transfer (Chandrasekhar,1960) the reflectance R and transmittance T of the atmosphere-surface system are written as:

$$R(\theta_0) = R^0(\theta_0) + r\tilde{T} \qquad (2)$$

$$T(\theta_0) = T^0(\theta_0) + r\tilde{R} \qquad (3)$$

where $r = \frac{\alpha T^0(\theta_0)}{1 - \alpha \tilde{R}}$, $T^0(\theta_0) = T^0_{dir}(\theta_0) + T^0_{dif}(\theta_0)$

In the above expressions R^0, T^0_{dir}, and T^0_{dif}; are the reflectivity and direct and diffuse transmissivities of the atmosphere. $\tilde{R}$ and $\tilde{T}$ are the spherical reflectivity and transmisivity, and α is the Lambertian surface albedo. Using the relationships $n_{SRF} = T(\theta_0)(1-\alpha)$ and $n_{TOA} = 1 - R(\theta_0)$, the SW net flux absorbed at the surface can be expressed as:

$$n_{SRF} = A + B\, n_{TOA} \qquad (4)$$

where $A = T^0(\vartheta_0) - B\left[1 - R^0(\vartheta_0)\right]$ and $B = \left(1 - \tilde{R}\right)/\tilde{T}$

A is a function of the atmosphere and the solar angle and *B* is only a function of the atmosphere, therefore, ASR can be estimated without explicit knowledge of the surface albedo. Equation 4 describes a linear relationship between TOA and surface net flux when *A* and *B* are constants or when they do not change much.

The atmospheric optical functions (reflectivity R^0; direct and diffuse transmissivity T^0_{dir}, T^0_{dif}; spherical reflectivity, $\tilde{R}$ and transmisivity, $\tilde{T}$) uniquely determine *A* and *B*. In the physical algorithm they are derived directly by interpolating the LUT values of the optical functions on the input solar zenith angle θ_0 and atmosphere parameters.

Three LUTs are generated for the physical algorithm. They are calculated for clear, water cloud and ice cloud scene types using the NASA Langley modified Fu-Liou radiative transfer code. As shown in Table 3-7 and Table 3-8, the clear-sky LUT of atmospheric optical functions are

functions of spectral bands, solar zenith angle, total precipitable water, ozone, surface elevation, aerosol optical depth at 0.55µm, and aerosol single scattering albedo (surrogate for aerosol type). Similarly, the LUT of cloudy sky optical functions depend on the spectral bands, solar zenith angle, total precipitable water, ozone, surface elevation, visible cloud optical depth, cloud radius and cloud top height.

Table 3-7. Extent of Clear-Sky Lookup Table

Parameter	Values	N
SW spectral Bands (µm)	0.175-0.224; 0.224-0.243; 0.243-0.285; 0.285-0.298; 0.298-0.322; 0.322-0.357; 0.357-0.437; 0.437-0.497; 0.497-0.595; 0.595-0.689; 0.689-0.794; 0.794-0.889; 0.889-1.042; 1.042-1.410; 1.410-1.905; 1.905-2.500; 2.500-3.509; 3.509-4.000	18
Cosine Solar Zenith Angle	.01, .025, .05, .08, .1, .15, .2, .3, .4, .5, .6, .7,.8, .9, 1.0	15
Natural log (Precipitable Water) [cm]	-4, -3, -2, -1, 0, 1, 2	7
Total Ozone [DU]	200, 350, 500	3
Surface Elevation [m]	-200, 0, 500, 1250, 4200.	5
Natural log(Aerosol Optical Depth)	-5, -4, -3, -2, -1, 0, 1	7
Aerosol Single Scattering Albedo at 0.55 µm (aerosol types)	0.9718, 0.955, 0.9429, 0.925, 0.8674 Oceanic, dust, urban, generic, absorbing	5

Table 3-8. Extent of Cloudy-Sky Lookup Table

Parameter	Values	N
SW spectral Bands (µm)	0.175-0.224; 0.224-0.243; 0.243-0.285; 0.285-0.298; 0.298-0.322; 0.322-0.357; 0.357-0.437; 0.437-0.497; 0.497-0.595; 0.595-0.689; 0.689-0.794; 0.794-0.889; 0.889-1.042; 1.042-1.410; 1.410-1.905; 1.905-2.500; 2.500-3.509; 3.509-4.000	18
Cosine Solar Zenith Angle	.01, .025, .05, .08, .1, .15, .2, .3, .4, .5, .6, .7, .8, .9, 1.0	15
Natural log (Precipitable Water) [cm]	-4, -3, -2, -1, 0, 1, 2	7
Total Ozone [DU]	200, 350, 500	3

Surface Elevation [m]		-200, 0, 500, 1250, 4200.	5
Natural log (Cloud Optical Depth)		2, -1, -0.5, 0, 0.5, 1.0, 1.5, 2.0, 2.5, 3, 4, 5	12
Cloud Effective Radius [μm]	Water Cloud	8, 12, 20, 30	4
	Ice Cloud	15, 30, 60, 90	
Cloud Top Height [m]		0, 3000, 5000, 8000, 14000	5

Calculation of the spherical quantities would require calculation of bidirectional reflectances and transmittances followed up with an integration of these quantities over the angles. It is not possible to calculate the bidirectional quantities from the modified Fu-Liou code since that code computes fluxes directly. Therefore, Equations (2) and (3) are used to calculate $\tilde{R}$ and $\tilde{T}$. For this the RTM is first run with a zero surface albedo that yields R^0 and T^0 directly, since *r* is zero in this case. Next, the RTM is run for the same atmosphere with a non-zero surface albedo (e.g., α = 0.3). Then the spherical reflectivity ($\tilde{R}$) and transmissivity ($\tilde{T}$) are calculated as:

$$\tilde{R} = \frac{T - T^0}{\alpha T} \quad \text{and} \quad \tilde{T} = \frac{R - R^0}{\alpha T} \qquad (5)$$

The absorbed SW radiation at the surface (ASR) is calculated as the product of n_{SRF} (calculated in Equation 4) and the extraterrestrial solar irradiance. The latter is obtained from the solar constant S_0 by correcting it for the actual sun-earth distance *d* (in astronomical units) and solar zenith angle θ_0, that is:

$$ASR = n_{SRF} \cos\theta_0 \frac{S_0}{d^2} \qquad (6)$$

3.4.2.2. The statistical algorithm

The method for retrieving the ASR applied in the statistical algorithm is based on a regression relationship between the TOA shortwave (0.2 - 4.0 μm) broadband albedo and ASR. For deriving the regression relationship ASR and TOA albedo are simulated from the modified version of the Fu-Liou RTM (Fu and Liou,1993). The simulations were performed for the variables shown in Table 3-7 and Table 3-8, along with seven surface albedos of black, ocean, crop, desert, sea ice, snow, and white (Figure 3-6).

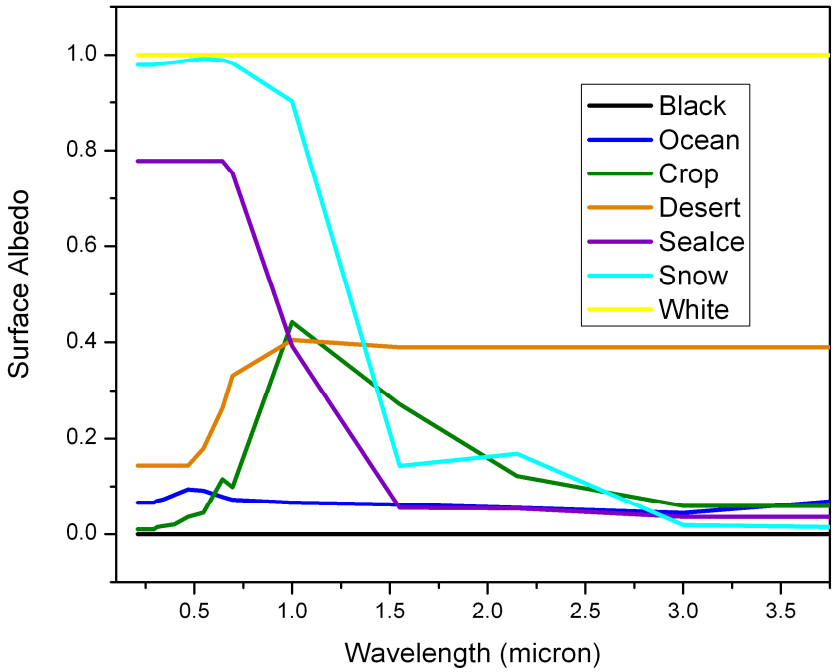

Figure 3-6. Surface albedos used in the simulation of data needed in the development of the statistical algorithm.

The linear regression between the simulated TOA albedo and ASR is derived for fixed solar zenith angles (θ_0) and fixed amounts of precipitable water (TPW). The fitting models are:

$$ASR = offset + slope\ R S_0 \cos\theta_0 \frac{d_0^2}{d^2}$$

$$\text{where} \quad offset = C_0 \cos(\theta_0) - C_1 \ln(TPW) - C_2, \qquad (7)$$

$$slope = C_3 \cos(\theta_0) - C_4 \ln(TPW) - C_5$$

R is TOA broadband albedo, S_0 is the solar constant, d and d_0 are the actual and mean Sun-Earth distances, respectively. The coefficients determined from the linear model are given in Table 3-9.

Table 3-9. Coefficients in linear model of statistical algorithm

C_0	C_1	C_2	C_3	C_4	C_5
1140.8	19.534	46.071	-0.0561	0.0078	1.095

3.4.2.3. NTB and ADM conversions

The mathematical formulas needed for converting the narrowband radiances observed by the satellite instrument to broadband albedo are described in the "GOES-R Advanced Baseline Imager (ABI) Algorithm Theoretical Basis Document for Downward Shortwave Radiation (Surface), and Reflected Shortwave Radiation (TOA), Ver. 2" and not repeated here.

3.4.3. Algorithm Output

All-sky absorbed shortwave radiation at surface (ASR) is the main output from the algorithm. Quality flags are produced to indicate product quality, algorithm path used, invalid or missing data, coast and snow/ice, retrieval with large solar angle (more than 70 degrees), or any unfavorable conditions. Table 3-10 lists the QC flag from the ABI ASR algorithm.

Table 3-10. Quality control flags.

No of Bits	Quality flag name	Bit Values	Cause & Effect
Product quality flag			
4	QC_GOOD	0	Processed, good quality
	QC_MARGINAL_PROC	1	Processed, see other process related flag
	QC_MARGINAL_INPUT	2	Processed, see other input related flag
	QC_NO_CONFIDENCE	3	No confidence (or fill)
Input data checking flags			
2	QC_INVALID_INPUT	0	All inputs are in valid range
		1	Invalid input; no retrieval from either physical or statistical algorithm
2	QC_LOW_MU	0	Solar zenith angle less than 70 degree
		1	Solar zenith angle larger than 70 degree
2	QC_LOW_MU2	0	Satellite zenith angle less than 70 degree
		1	Satellite zenith angle larger than 70 degree
2	QC_POLARNIGHT	0	not polar night
		1	Polar night; outputs are set to zero
Input data resource flags			
2	QC_SNOW/ICE	0	No snow/ice input
		1	Snow/ice is present
2	QC_CLIM_TPW	0	Total precipitable water is from ABI retrieval
		1	Total precipitable water is from climatology
2	QC_COAST*	0	Not coastal region
		1	Coastal region

Processing path flag			
2	QC_STAT	0	Retrieval is from Physical algorithm
		1	Retrieval is from Statistical algorithm
Processing related flags			
4	QC_INVALID_SFCALB(NSCN)	0	Calculated surface albedo is valid when physical algorithm is used
		1	Calculated surface albedo is out of range in clear sky scene
		2	Calculated surface albedo is out of range in water cloud scene
		3	Calculated surface albedo is out of range in ice cloud scene
4	QC_NO_NTBREF(NSCN)	0	Broadband reflectance is in valid range
		1	Unable to convert narrowband reflectance to valid broadband TOA reflectance in clear sky; outputs are set to missing values
		2	Unable to convert narrowband reflectance to valid broadband TOA reflectance in water cloudy sky; outputs are set to missing values
		3	Unable to convert narrowband reflectance to valid broadband TOA reflectance in ice cloudy sky; outputs are set to missing values
4	QC_NO_ANGCOR(NSCN)	0	Angular correction is performed
		1	No angular correction in clear sky; output is set to missing value
		2	No angular correction in water cloudy sky; output is set to missing value
		3	No angular correction in ice cloudy sky; output is set to missing value
2	QC_FAIL_PHYS	0	Valid ASR estimates from physical algorithm
		1	Physical algorithm retrieval failed; Estimated ASR is out of expected valid range (0-1200 Wm^{-2}) ; outputs are set to missing values
2	QC_FAIL_STAT	0	Valid ASR estimates from statistical algorithm
		1	Statistical algorithm retrieval failed; Estimated ASR is out of expected valid range (0-1200 Wm^{-2}) ; outputs are set to missing values

Internal products include the broadband TOA albedo and calculated surface albedo associated with each scene type when the physical algorithm is used; and scene average TOA albedo when the statistical algorithm is used. These will be available for diagnostic purposes.

Metadata includes statistics of ASR such as minimum, maximum, mean, and standard deviation of the products. Total number of pixels for which retrieval was attempted and number of pixels with local zenith angles larger than 70º are held in metadata.

4. Test Data Sets and Outputs

4.1. Simulated/Proxy Input Data Sets

This section describes the test data sets used to characterize the performance of the algorithm and quality of the data product(s), including the breadth of the domain (typical versus stressing states) used in the analysis and assessment.

As described below, the data used to test the ABI ASR algorithm included MODIS observations. The MODIS data (from both Terra and Aqua) are from March 2000 to June 2006 and collocated around ten ground stations from the Surface Radiation Budget Network (SURFRAD) and the Climate Monitoring and Diagnostics Laboratory (CMDL) surface radiation monitoring project.

4.1.1. MODIS Data

MODIS proxy data used for testing the ABI ASR algorithm include L1B SW narrowband reflectances at 1-km resolution (channel mapping is shown in Table 4-1); Level 2 products of aerosol optical depth; cloud optical depth, size, phase, height; total precipitable water, ozone; and cloud and snow mask. Data within 5 km square regions centered on 10 ground stations (Table 4-2) are averaged. The retrieved ASR is compared with ground flux measurements.

Table 4-1. Channel mapping between ABI and MODIS.

ABI Channel	MODIS Channel
Channel 1: 0.47 µm	Channel 3: 0.47 µm
Channel 2: 0.64 µm	Channel 1: 0.66 µm
Channel 3: 0.86 µm	Channel 2: 0.86 µm
Channel 4: 1.38 µm	Channel 26: 1.38 µm
Channel 5: 1.61 µm	Channel 6: 1.64 µm
Channel 6: 2.26 µm	Channel 7: 2.13 µm

Table 4-2. Ground stations used for validating retrieved ASR from MODIS proxy data

Station Label	Station Name	Network	Latitude	Longitude	Elevation [m]
BON	Bondville, IL	SURFRAD	40.05	-88.37	213
DRA	Desert Rock, NV	SURFRAD	36.63	-116.02	1007
FPK	Fort Peck, MT	SURFRAD	48.31	-105.10	634
GWN	Goodwin Creek, MS	SURFRAD	34.25	-89.87	98
PSU	Penn State, PA	SURFRAD	40.72	-77.93	376
SXF	Sioux Falls, SD	SURFRAD	43.73	-96.62	473
TBL	Table Mountain, CO	SURFRAD	40.13	-105.24	1689
COV	Chesapeake Bay Light Tower, MD	COVE	36.90	-75.71	30
E13	Lamont, OK	ARM	36.61	-97.48	318
BOU	Boulder Tower, CO	CMDL	40.05	-105.01	1584

4.2. Output from Simulated/Proxy Inputs Data Sets

ASR is retrieved from MODIS proxy data from March 2000 to June 2006. The retrievals are then compared with ground measurements of the same quantity from SURFRAD and CMDL, and statistics to characterize the performance of the algorithm are generated.

4.2.1. Precision and Accuracy Estimates

This section describes the predicted algorithm performance and quality of the products at a level of detail appropriate for the current algorithm maturity given instrument performance is as required.

Evaluation of the ASR products retrieved from the ABI ASR algorithm is performed by comparison with various ground measurements. Following the F&PS definition, bias and one-sigma standard deviation is calculated for all retrievals as well as the typical low, medium and high value ranges to assess the retrieval accuracy and precision.

The performance of both physical and statistical algorithms is predominantly determined by the uncertainties associated with the spectral and angular conversion used for estimating the broadband TOA albedo from the narrowband ABI reflectances. Retrieval performance is also influenced by the uncertainty of the input ABI products. Thus it is anticipated that low quality of ASR would be associated with conditions unfavorable for the cloud and aerosol retrievals, such as over cold bright surface, oblique viewing geometry, and coastal regions etc. It is noted that differences in observing geometry and spatial scales of satellite retrievals and ground/TOA observations can make the validation difficult.

Based on the validations performed so far, the overall accuracy of retrieved ASR is estimated to be within ~4% with the largest errors appearing at the extreme (low and high) value ends. This feature can be largely attributed to the systematic over-/under-estimation of the cloud fraction

when the "truth" is measured under clear-sky/overcast conditions. The overall precision of retrieved ASR is estimated to be within 24%. Figure 4-1 shows the evaluation of retrieved ASR from MODIS data against the ground measurements. The dependence of retrieval error on the magnitude of observed values is clearly demonstrated.

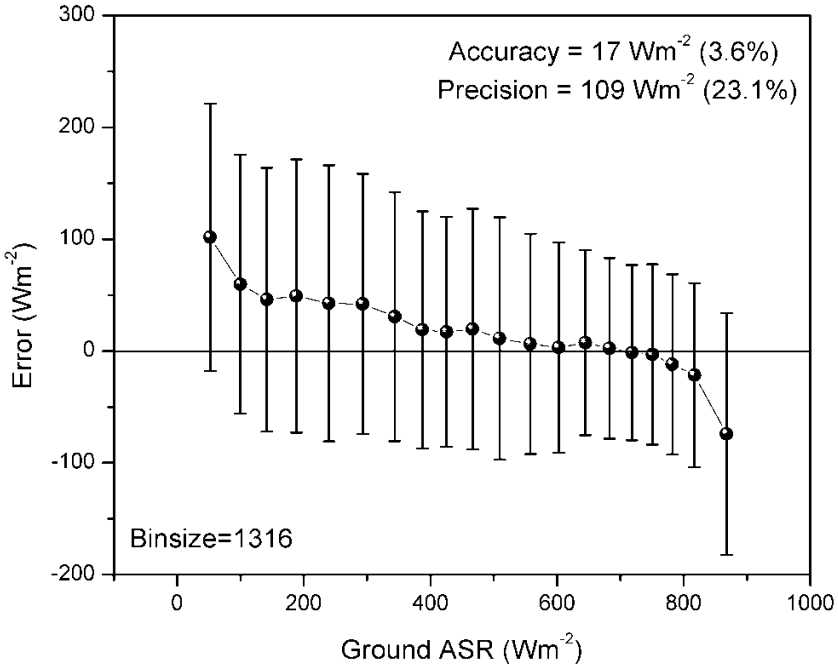

Figure 4-1. Error of ASR retrieved from MODIS proxy data as a function of ground measurements. Vertical bar represents the standard deviation of retrieval errors within each bin.

4.2.2. Error Budget

Accuracy and precision of ASR are estimated for MODIS proxy data. Table 4-3 lists the validation results as well as the F&PS requirements. Proposed requirements are defined at three typical value ranges based on the earlier validation practice with the ABI DSR/RSR algorithm.

The current validation with MODIS data demonstrates that the performance of ABI ASR algorithm satisfies the accuracy requirements. It should be noted that, given the wide range of ASR values, assessment of performance depends on the validation samples from which the statistics are derived. Validation performed at different locations, distinct diurnal phase or using retrieval inputs from different sources could generate different accuracy and precision values for the same algorithm.

Table 4-3. Accuracy and precision of ASR estimation with MODIS data

ASR	F&PS	Validation	F&PS	Validation

Measurement (Wm^{-2})	Requirement Accuracy	with MODIS (Accuracy)	Requirement Precision	with MODIS (Precision)
Low (100)	±90	60	75	116
Middle (400)	±45	19	95	106
High (800)	±55	-12	75	87
Overall		17		109

Primary sources of error in ASR estimation is due in part to uncertainties in input ABI reflectances, input ABI products, cloud mask, spectral and angular conversions, aerosol and cloud models in LUT, and ancillary data. The results also include the uncertainty of matching satellite retrievals with point ground measurements; the errors at the large and small value ends can be largely attributed to the inconsistent cloud fraction in the satellite and ground data.

Estimation of errors is done by perturbing the different sources by known amounts and comparing the results to those from the unperturbed values. Table 4-4 summarizes the degree of perturbation in each input parameters (based on F&PS version 2.0) in each input parameters. The response of the ABI ASR algorithm to those inputs is shown in Figure 4-2. The algorithm response is less than 5 Wm^{-2} except for TOA albedo. Errors in TPW and ice cloud optical depth cause the largest errors in ASR estimation after TOA albedo. Effect of change in water cloud optical depth is small and not shown in Figure 4-2.

Table 4-4. Preparation of perturbed data in each input parameters (F&PS version 2.0)

Input	TPW	Ozone	AOD	Cloud mask	Water Cloud Radius	Ice cloud radius	Water cloud OD	Ice cloud OD	TOA albedo
Product Accuracy	±10%	±8%	±30%	±11%	±4 μm	±10 μm	±8%	±30%	±14%

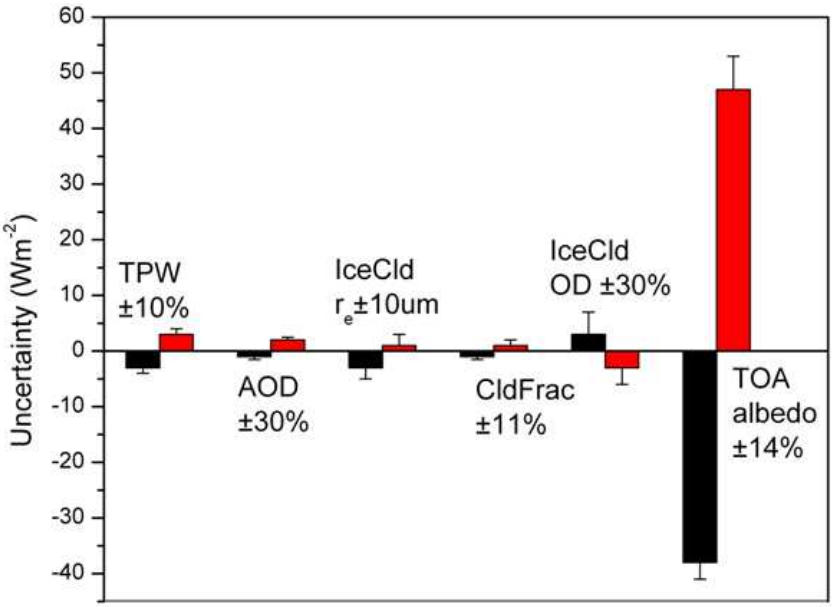

Figure 4-2. Errors of ABI ASR algorithm response to the perturbed input parameters.

4.2.3. Framework Validation

To be completed after TRR

5. Practical Considerations

5.1. Numerical Computation Considerations

Solution of the radiative transfer is represented in LUT. The LUT approach uses pre-calculated values of spectral atmospheric transmittances, reflectances, spherical transmittance and albedo. This makes calculations relatively fast.

5.2. Programming and Procedural Considerations

The retrieval is carried out on a grid scale, and all inputs should be consistent with the same spatial resolution. The algorithm requires calibrated and geo-located ABI reflectances, ABI cloud mask and snow/ice mask, water vapor and ozone amount; aerosol, and cloud products as ABI dynamic input. Mapping processes for static ancillary (e.g. surface elevation, surface type) can be processed offline. The programming design uses modules, providing the flexibility for ease upgrades.

5.3. Quality Assessment and Diagnostics

The following procedures are used for diagnosing the performance:

- Monitor the percentage of daytime pixels with valid retrievals. This number is compared to the "astronomically" possible value.
- Processing path flag indicates physical and statistical algorithm.
- Flag any situation which might degrade the retrieval quality (input data resource flags to check if climatology is used due to missing input etc.; processing related flags to indicate internal retrieval falls out of LUT range etc.)
- Evaluate individual quality flags and assess the overall quality.

.

5.4. Exception Handling

The ABI ASR algorithm checks the validity of each input and situations causing the unintentional abort of the retrieval. List of exceptions is shown in Table 5-1.

Table 5-1 Exceptions handled in algorithm

Exception	Detection	Handling
Invalid Input	Inputs out of valid range	No retrieval
Low solar position	SZA > 70^o	Degrade the quality flag
Snow/ice present	Snow fraction > 0	Degrade the quality flag
Coastal region	Checking coast mask	Degrade the quality flag
Missing water vapor input	Input set as missing	Replaced with climatology
Missing column ozone input	Input set as missing	Retrieval with statistical algorithm
Missing water cloud optical depth input	Input set as missing	Retrieval with statistical algorithm
Missing water cloud radius input	Input set as missing	Retrieval with statistical algorithm
Missing water cloud height input	Input set as missing	Retrieval with statistical algorithm
Missing ice cloud optical depth input	Input set as missing	Retrieval with statistical algorithm
Missing ice cloud radius input	Input set as missing	Retrieval with statistical algorithm
Missing ice cloud height input	Input set as missing	Retrieval with statistical algorithm
Physical algorithm retrieval failed	Illegal numerical computation	Quit retrieval
Statistical algorithm retrieval failed	Illegal numerical computation	Quit retrieval
Polar night	Checking time and location	No retrieval
Unable to convert	TOA albedo < 0	Quit retrieval

reflectances to TOA albedo for clear scene		
Unable to convert reflectances to TOA albedo for water cloud scene	TOA albedo < 0.	Quit retrieval
Unable to convert reflectances to TOA albedo for ice cloud scene	TOA albedo < 0.	Quit retrieval
Invalid calculated surface albedo for clear scene	Calculated surface albedo from input is out of range	Degrade the quality flag, physical algorithm
Invalid calculated surface albedo for water cloud scene	Calculated surface albedo from input is out of range	Degrade the quality flag, physical algorithm
Invalid calculated surface albedo for ice cloud scene	Calculated surface albedo from input is out of range	Degrade the quality flag, physical algorithm
Unable to calculate flux	Illegal numerical computation	Quit retrieval

5.5. Algorithm Validation

5.5.1. Pre-Launch Phase Activities

During the pre-launch phase of the GOES-R program, validation of the ABI ASR algorithm has two stages. First, the two components of the ABI ASR algorithm (the physical and the statistical algorithm) are evaluated independently (as separate algorithms) with common data (SEVIRI, CAVE, and MODIS data) that supply the input needed for both the physical and statistical algorithms. In the second stage the combined algorithm is tested with the common data set (MODIS) used in the first stage. This stage tests the implementation of the combined algorithm with the expectation that the statistics will be similar to those obtained in the first stage. The data sets used in these stages are described below in some more details.

- SEVIRI observations from two SW channels (0.63 and 0.86 µm) with a spatial resolution of 3 km and a temporal resolution of 1 hour. Pixel-level SEVIRI data are averaged into ½ degree equal-angle grids to use atmospheric information retrieved from the ABI DSR/RSR algorithm. Grouping and averaging of SW reflectance is carried out separately for clear and cloudy scenes. The SEVIRI data covers four seasonal months (Jan., Apr., Jul., and Oct.) in 2006 and 2008. Measurements at two BSRN stations (TOR and PAY) are used for evaluating the retrieved ASR.
- CERES ARM Validation Experiment (CAVE) data with satellite-derived TOA CERES fluxes. The CAVE data include broadband TOA flux, therefore, spectral and angular transformation of narrowband reflectances are not necessary. The CAVE data also include the reference data in the form of ground-measurements of surface flux from nearly 30 sites of ARM, BSRN, SURFRAD, and CMDL from 2000 to 2006.

- MODIS proxy data of SW narrowband reflectances at 1km resolution, atmospheric products, and cloud/snow masks with ground measurements from ten stations of SURFRAD, CMDL, and ARM. To approximate the horizontal spatial resolution of the ASR product, pixel-level MODIS data are averaged into 5-km square regions. Grouping and averaging of SW reflectance is carried out separately for clear and cloudy scenes.

In addition to the above data, ideally, the following proxy data could be used for algorithm development and testing during the pre-launch phase:

- A 12 month collocated dataset of GOES radiances. The corresponding ground and ancillary data that include upward and downward SW fluxes measured at the surface at SURFRAD sites and from four buoys, climatological (NCEP/ECMWF) and/or GFS-based total column amounts of ozone and water vapor.
- A set of hourly SEVIRI images per month for four seasonal months.
- Four seasonal months of MODIS radiances for at least 10 MODIS granules. The selected MODIS granules include at least one surface site.
- Four sets of model simulated ABI proxy data for daytime hours representing the four seasons.

A more detailed evaluation of the algorithm performance is conducted in the evaluation phase of the AWG project. Results from this evaluation that includes dependence of accuracy and precision on seasons, regions, input parameters will be described in the Validation Report, along with the techniques and tools developed for the validation.

5.5.2. Post-Launch Phase Activities

During the post-launch period validation, methodologies and tools developed and tested during the pre-launch period will be applied to actual ABI ASR retrievals. Concurrent VIIRS and CERES on JPSS platforms and ABI data will be collected. The ABI algorithm will be run with all three data types, and the results will be compared with each other and with ground data. Running the algorithm with VIIRS (similar to MODIS) will help in relating the pre-launch validation to that in the post-launch phase relatively quickly without the need for waiting for the collection of long-term data.

The validation results will be used to identify algorithm shortfalls. Refined algorithm will be developed and tested using accumulated reference and ABI data. Refinements will be sent to the GOES-R System Prime Contractor for integration.

5.5.3. Correlative Data Sources

The ground-based data provide completely independent observational data to which the comparable satellite-derived values can be validated and otherwise evaluated. These observations are available from multiple NOAA operated sites (SURFRAD and other ESRL/GMD sites) throughout the algorithm development, prelaunch, and post launch periods.

The NASA/CERES project generates state-of-the art estimates of TOA and surface fluxes. The CERES product includes a suite of retrievals from algorithms of varying complexity. These data are used for both development and validation of the ABI ASR algorithm. Similar datasets are expected to be available from CERES follow-up instruments onboard the JPSS satellites.

6. ASSUMPTIONS AND LIMITATIONS

6.1. Performance

The following assumptions have been made in developing and estimating the performance of the algorithm.

1. Surface is Lambertian.
2. Calibrated reflectances in ABI SW channels are ready.
3. High quality static ancillary data are available at the grid level.

Limitations that could affect the retrieval performance are:

1. Quality of the ASR will critically depend on the quality of ABI cloud and aerosol products.
2. Quality of NTB and ADM, and those of the ABI reflectances have significant impact on the quality of ASR.
3. Unknown spectral shifts in some channels will cause biases in the clear-sky RTM calculations that may impact the performance of the NTB.
4. RT model is 1-D; 3-D effects, which can be significant at the 5-km scale, are not considered.
5. Retrievals over snow and ice (cloud identification, aerosol retrieval); high loading of absorbing aerosol (aerosol optical depth will be off); coastal region (highly inhomogeneous surface); and twilight are inherently more difficult.

6.2. Assumed Sensor Performance

It is assumed that the ABI sensor will meet its current specifications. However, the SRB will be dependent on the following instrumental characteristics.

- Unknown spectral shifts in some channels will cause biases in the TOA albedo estimation and then impact the ASR retrievals.

6.3. Pre-Planned Product Improvements

6.3.1. Update NTB conversion

The currently implemented NTB conversion accounts only for the solar angle. Including the dependence on viewing and azimuth angles (even though they had been found to produce

inferior results using the limited simulation for NTB) should be revisited. Possible elevation dependence of NTB should also be investigated and incorporated in the update.

6.3.2. Update LUT

The current LUT uses cloud models that are different from the ones used by the ABI Cloud Team. There is a possibility to update the LUT to be consistent with the ABI cloud retrievals. In addition, a common RTM is proposed to be used by all ABI algorithm development groups to increase the consistency among various ABI products. If such common RTM has the capability to calculate broadband SW fluxes, the LUT in the ABI ASR algorithm must be re-calculated.

7. REFERENCES

Cess, R.D., Dutton, E.G., Deluisi, J.J., & Jiang, F. (1991). Determining surface solar absorption from broad-band satellite measurements for clear skies - Comparison with surface measurements. *Journal of Climate, 4*, 236-247

Cess, R.D., & Vulis, I.L. (1989). Inferring surface solar absorption from broadband satellite measurements. *Journal of Climate, 2*, 974 - 985

Chandrasekhar, S. (1960). Radiative Transfer, Dover, Mineola, N.Y.

Fu, Q., & Liou, K.N. (1993). parameterization of the radiative properties of cirrus clouds. *Journal of the Atmospheric Sciences, 50*, 2008-2025

Kim, H.Y., & Liang, S.L. (2010). Development of a hybrid method for estimating land surface shortwave net radiation. *Remote Sensing of Environment, in revision*

Laszlo, I., Heidinger, A., Tarpley, J.D., Jelenak, A., & Pinker, R.T. (2004). High spatial resolution shortwave radiative fluxes from GOES. *International Radiation Symposium*, edited, Busan, Korea

Laszlo, I., & Pinker, R.T. (1994). On the relationship between shortwave net radiative fluxes at the top of the atmosphere adn at the surface. *Eighth Conference on Atmospheric Radiation, Nashiville, TN, January 23-28, Amer. Meteor. Soc.*, 532-533

Laszlo, I., & Pinker, R.T. (2002). Shortwave radiation budget of the Earth: Absorption and cloud radiative effects. *Időjárás, Quarterly Journal of the Hungarian Meteorologial Service, 106*, 189-205

Li, Z.Q., Leighton, H.G., Masuda, K., & Takashima, T. (1993). estimation of sw flux absorbed at the surface from toa reflected flux. *Journal of Climate, 6*, 317-330

Masuda, K., Leighton, H.G., & Li, Z.Q. (1995). A new parameterization for the determination of solar flux absorbed at the surface from satellite measurements. *Journal of Climate, 8*, 1615-1629

Pinker, R.T., Ewing, J.A., & Tarpley, J.D. (1985). the relationship between the planetary and surface net-radiation. *Journal of Climate and Applied Meteorology, 24*, 1262-1268

Pinker, R.T., Frouin, R., & Li, Z. (1995). A review of satellite methods to derive surface shortwave irradiance. In (pp. 108-124)

Pinker, R.T., & Laszlo, I. (1992). Modeling surface solar irradiance for satellite applications on a global scale. *Journal of Applied Meteorology, 31*, 194-211

Pinker, R.T., & Tarpley, J.D. (1988). The relationship between the planetary and surface net-radiation - An update. *Journal of Applied Meteorology, 27*, 957-964

Ramanathan, V. (1986). Scientific use of surface radiation budget data for climate studies. Surface Radiation Budget for Climate Studies *NASA Ref. Publ. (J. T. Suttles and G. Ohring, Eds.)*, 132 pp.

Rossow, W.B., & Zhang, Y.C. (1995). Calculation of surface and top of atmosphere radiative fluxes from physical quantities based on ISCCP data sets . 2. Validation and first results. *Journal of Geophysical Research-Atmospheres, 100*, 1167-1197

Schmetz, J. (1993). Relationship between solar net radiative fluxes at the top of the atmosphere and at the surface. *Journal of the Atmospheric Sciences, 50*, 1122-1132

Tang, B.H., Li, Z.L., & Zhang, R.H. (2006). A direct method for estimating net surface shortwave radiation from MODIS data. *Remote Sensing of Environment, 103*, 115-126

Wielicki, B.A., Barkstrom, B.R., Harrison, E.F., Lee, R.B., Smith, G.L., & Cooper, J.E. (1996). Clouds and the earth's radiant energy system (CERES): An earth observing system experiment. *Bulletin of the American Meteorological Society, 77*, 853-868

Zhang, Y.C., Rossow, W.B., Lacis, A.A., Oinas, V., & Mishchenko, M.I. (2004). Calculation of radiative fluxes from the surface to top of atmosphere based on ISCCP and other global data sets: Refinements of the radiative transfer model and the input data. *Journal of Geophysical Research-Atmospheres, 109*